Native gold from volcanic gases at Tolbachik 1975–76 and 2012–13 Fissure Eruptions, Kamchatka

Ilya Chaplygin *[1], Marina Yudovskaya [1], Lidiya Vergasova [2], Andrey Mokhov [1]

[1] Institute of Geology of Ore Deposits, Petrography, Mineralogy and Geochemistry, Russian Academy of Sciences, Moscow, Russia

[2] Institute of Volcanology and Seismology, Far East Division, Russian Academy of Sciences, Petropavlovsk-Kamchatsky, 683006 Russia

*corresponding author ichap@rambler.ru

Abstract

Aggregates and euhedral crystals of native gold were found in sublimates formed during New Tolbachik Fissure Eruption in 2012–2013 (NTFE). Gold-bearing sublimate samples were taken from a red-hot (690 °C) degassing fracture in the roof of an active lava tunnel 1.5 km from active Naboko cinder cone in May 2013. The gas condensate collected at 690 °C in this site contains 16 ppb Au, 190 ppb Ag and 1180 ppm Cu compared to 3 ppb Au, 39 ppb Ag and 9.7 ppm Cu in the condensate of pristine magmatic gas sampled at 1030 °C. The 690 °C volcanic gas is most likely a mix of magmatic gas and local snow buried under the lava flows as indicated by oxygen and hydrogen isotope compositions of the condensate. The lower-temperature gas enrichment in gold, copper and chlorine is resulted from evaporation of the 690 °C condensate during forced gas pumping at sampling. Native gold was also found in fumarolic encrustations collected from caverns in basalt lava flows with temperature up to 600 °C in June 2014, in a year after eruption finished.

The native gold precipitation in newly formed Cu-rich sublimates together with the well known gold occurrences in cinder cones of 1975–1976 Large Tolbachik Fissure Eruption manifest a transport capability of oxidized volcanic gas.

Keywords

2012–13 Tolbachik eruption, native gold, fumarole, volcanic gas, 1975-76 Tolbachik Eruption

1. Introduction

Analyses of Au content in fumarole vapor along with fluid inclusion data from porphyry-type ore deposits demonstrate that significant quantities of Au may be scavenged by magmatic volatile phases. Gold contents reported in fumarolic condensates may vary from 0.01 ppb to 32

ppb (Hedenquist et al. 1994; Williams-Jones et al., 2005) whereas Au content in vapor-rich inclusion from magmatic-hydrothermal mineralization reaches 10 ppm revealing stronger partitioning into low-salinity aqueous vapor with respect to co-existing brine (Ulrich et al., 1999; Kouzmanov and Pokrovski, 2012; Pokrovski et al., 2014). Therefore, Au concentrations in condensates of volcanic gases are much lower than in hydrothermal fluids trapped in inclusions and comparable with Au contents in igneous rocks (0.23 ppb according to Morgan et al., 1978) and the upper continental crust (1.5 ppb after Rudnick and Gao, 2004). Nevertheless, Au minerals were reported on several volcanoes from sublimates enriched with other volatile ore elements (i.e. Henley and Berger, 2013). Gold particles 20–60 μm in size were found in plume aerosols of Mount Erebus in Antarctica as well as in snow samples nearby this volcano (Meeker et al., 1991). Crystals of native gold occur among precipitates on inner walls of quartz tubes inserted in fumarolic vents with temperature of 800ºC on Colima volcano, Mexico (Taran et al., 2000). Rare particles of Au–Cu–Ag alloys as well as minute crystals of native gold were described at La Fossa crater, Italy (Fulignati and Sbrana, 1998) and in fumarolic products of Kudriavy volcano, Iturup Island, Kuriles (Korzhinsky et al., 1996; Yudovskaya et al., 2006). Extremely small crystals of gold alloys and gold-bearing compounds less than 1 micron in size were detected in quartz tube sublimates from Erta Ale, Ethiopia (Zelenski et al., 2013). The most abundant and amazing fumarolic gold was discovered in 1979 on cinder cones of Large Tolbachik Fissure Eruption (LTFE) occurred on Kamchatka in 1975–1976 (Vergasova et al., 1982; 2001).

Here we report on native gold found in sublimate encrustations formed during New Tolbachik Fissure Eruption in 2012–2013 (NTFE) which lasted from 27.11.2012 until 28.08.2013 and produced 0.55 km^3 of basalt (Belousov et al., this volume). Gold-bearing sublimate samples were taken from a red-hot (690°C) passively degassing fracture in the roof of an active lava tunnel approximately 1.5 km from active Naboko cinder cone in May 2013 (Fig. 1). Native gold was also found in fumarolic encrustations collected from caverns in lava flows still heated up to 600 °C in June 2014. In contrast to the spectacular native Au from LTFE visible with naked eye, particles of native gold were not observed visually in the NTFE samples. Individual crystals and aggregates of gold were extracted from heavy water-insoluble fractions as well as were identified on the surface of fumarolic minerals under scanning electron microscope (SEM).

Findings of native gold and Au-bearing alloys in immediate products of volcanic eruptions are of great interest since it proves transport and deposition of gold directly from gas phase. In this study, we discuss process of post- and syn-eruptive gold deposition as seen in the NTFE and

provide comparative detailed observations on native gold from the previous LTFE to highlight the general characteristics of fumarolic gold deposition from oxidized volcanic gas.

2. Methods and samples

High-temperature gases of the 2012-2013 NTFE were sampled in Giggenbach bottles filled with ammonia solution (Giggenbach, 1975; Sortino et al., 2006). Gas condensates were collected via water cooled glass condenser. The temperature of the gas was measured with a K-type thermocouple. A one-meter long quartz tubes 1 inch in diameter was inserted into the high-temperature vent at the gas sampling site for 2 days to study experimental sublimates inside the tube. The tube was sealed after sampling.

The LTFE sublimate samples were collected during field work in 1990 at the Cone II of the Northern Breakthrough. Rock samples with sublimates at the NTFE were collected during two field expeditions in 2013 and 2014. The samples were packed in plastic wrap when cooled. In the lab the samples and the glass tube were put in a glass jar with distilled water for 2–5 days to dissolve soluble precipitates. The samples were carefully rinsed with distilled water, heavy fractions were separated using tribromomethane and cleaned with ethanol. Native gold was found in two large samples Tol0313 and Tol2714, which have been split into several pieces and then treated separately.

Trace element content in gas condensate was analyzed by ICP-MS with an Element-II at IGEM RAS (Moscow). Detailed description of sampling and analytical procedures is given by Chaplygin et al. (submitted).

Mineral compositions were determined from untreated fragments of sublimates and separated individual grains on carbon tape without coating, using a scanning electron microscope (SEM) Jeol-5610 LV with an energy dispersive spectrometer at the Belov Laboratory of Crystallochemistry IGEM RAS (Moscow). Back-scattered electron (BSE) images were obtained with the same electron microscope. The compositions of selected grains were measured in polished blocks with a Jeol JXA 8200 microprobe at IGEM RAS, using primary and secondary mineral standards. The precision of measurement were better than 2–3 relative %.

3. Tolbachik native gold occurrences

3.1. LTFE 1975–76 cinder cones

The Large Tolbachik Fissure Eruption of 1975–1976 formed several cinder cones (Large ..., 1984). Cones I and II of Northern Breakthrough (Fig. 1) are still hot at the top and emitting volcanic gases with temperature up to 440 °C from circle cracks along the crater rims. Gases are air- and CO_2-rich and believed to obtain their temperature due to secondary heating (oxidation of

Fe^{2+}) inside the cones (Large ..., 1984). These gases cause intense alteration of pyroclastic material in the upper parts of the cones forming brick-red colored rocks partly cemented by cryptocrystalline ralstonite $NaMg[Al(F,OH)_6]*H_2O$ and other oxyhalogenides, halogenides, sulfates and oxysulfates with numerous Cu compounds formed in pores and cavities (Vergasova et al., 2001; Karpov et al., 2003) (Fig. 2A).

Samples with visible gold were firstly taken in 1979 on Cone II at depth of 20–30 cm (Vergasova et al., 1982). Native gold, comprising pure Au (<3 wt.% of Ag in some cases), was found later in 1985, 1990, 1998 (Cone II), and in 1996 (Cone I), (Vergasova et al., 2001, Karpov et al., 2003). Figure 2B shows surface of altered basaltic cinder (sample Tol 76-7/90) covered by numerous crystals of native gold and demonstrates their abundance. Some of the particles are partially buried under fumarolic precipitates while others are completely exposed on the surface of the crust (Fig. 2 C–F). Native gold from LTFE cones typically forms trigonal and hexagonal plates up to 0.3 mm in size with signs of skeletal growth (Fig. 3). It also occurs as smooth aggregates of rounded elongated and isometric grains with relics of faces (Fig. 4). The reason for such a morphology could be either their growth from gas depleted in Au or following partial dissolution, or both. However, angular euhedral crystals of prismatic (Fig. 5A–C) and octahedral (Fig. 5D) habit are also very abundant. Native gold is closely associated with melanothallite Cu_2OCl_2 (Fig. 5E, F), tolbachite $CuCl_2$, euchlorine $KNaCu_3O(SO_4)_3$, chalcocyanite $CuSO_4$, aphthitalite $(K,Na)_3Na(SO_4)_2$, hematite, and other fumarolic minerals.

The highest Au content (143 ppm) was measured by ICPMS in the bulk sample of altered volcanic rocks with Cu-chloride mineralization although Na-, Al-, and Mg-fluoride mineralization was also rich in gold (101 ppm) (Karpov et al., 2001). Gold enrichment was observed locally at cinder cones in restricted areas that have been affected or are being affected by post-eruptive degassing. Direct measurements showed that native gold deposition may take place in the temperature ranges of 280–320 ^oC on Cone I, 400–625 ^oC and 180–260 ^oC on Cone II (Vergasova et al., 2001).

3.2. 2012–2013 NTFE lava flows

The samples of fumarolic precipitates (Tol 0313) were collected near a small degassing fracture glowing at ~2 m depth, 1.5 km to the south from Naboko cone in May 2013 (Fig. 1). At the time of sampling lava was flowing beneath the roof of the flow and gases came from the lava tube. Vapors circulated inside the fractures likely represent a mixture of volcanic gases and meteoric water, where the latter mostly originated from a snow pack buried under the flowing lava (Edwards et al., 2014). Volcanic condensate with a gas temperature of 690^oC was sampled from this site (Chaplygin et al., submitted). The gas sampling at the 690 ^oC point was

unsuccessful because of very slow discharge and high air contamination. Rock samples represented fragments of very porous basaltic lava crust ~5 cm thick, coated by light-green chloride-sulfate mineralization deposited from gas (Fig. 6A, B). Host pahoehoe basalt has vitreous texture with rare plagioclase phenocrysts and minute microlites of clinopyroxene.

Three native gold particles were found under a binocular microscope among a pile of sugar-white anglesite ($PbSO_4$) crystals in the heavy separate, and these were put on carbon tape for a SEM study. The most abundant mineral in the heavy fraction is anglesite; tiny spheres of hematite and crystals of galena are present. Three flat particles up to 100 microns in size were confirmed to be aggregates of native gold; also detected were free platy triangular and hexagonal gold crystals less than 2 microns in size. Each aggregate looks like a planar network composed of accreted smooth isometric and flattened crystals 1–5 microns (up to 10 microns) in size (Fig. 6 C, D). The surface of gold crystals locally contains fingerprints of dissolved minerals that have been in the intergrowth with native gold. After dissolution in water, the only mineral observed in the intergrowth with native gold was anglesite (Fig. 7A). However, SEM study of the untreated sample Tol 0313 reveals numerous tiny crystals of native gold among Cu sulfates. Encrustations are mostly composed of complex K-Cu sulfates with predominant cyanochroite $K_2Cu(SO_4)_2*6H_2O$ based on morphology, EDS spectrum, EDS semiquantitative analysis and the element proportions. Cyanochroite occurs as greenish-blue tabular crystals up to 5 mm long arranged in druse-like aggregates and rosettes. The surface of the sulfate crystals is porous with signs of dissolution. Particles of native gold and anglesite occupy small cavitites or intergrow with cyanochroite (Fig. 7B).

Following this finding, 4 more samples with sulfate incrustations and precipitates from a quartz tube were washed and studied under SEM. Native gold was not found in the samples with white and yellowish incrustations, which did not show typical green coloration by Cu minerals and were rich in Fe, Ca and K-Na sulfates and hydrosulfates. The inner surface of the quartz tube inserted for 2 days in the vent with the gas temperature of 690^{o}C was covered with a thick layer of yellow-green sublimates, which were mostly composed of soluble Cu sulfates. Insoluble remains of the tube sublimates did not contain Au minerals and did not carry any heavy fraction except for micrograins of ilmenite and titanomagnetite likely brought as aerosol from basaltic matrix.

Numerous fine gold crystals 0.1–2 microns in size were observed on the surface of crystals of an unidentified Cu-Fe borate from the sample Tol 2714 taken from the mouth of a red-hot crack in basalt flow in June 2014. The basalt substrate was covered by a thick crust of white sublimates with visible black opaque platelets of tenorite (CuO) and the semitransparent brown tabular Cu-Fe borate (Fig. 7C-E). This mineral has been firstly determined under SEM as an

unknown complex Cu-Fe oxide. From microprobe analysis of a polished grain the mineral contains (wt. %): 1.2 Al_2O_3, 18.13 Fe_2O_3, 4.67 TiO_2 and 60.04 CuO with a total of 84.04 wt. % (analyst I. Griboedova, IGEM RAN) indicating a Cu/Fe atomic ratio of ~2/1 and suggesting the presence of volatile or light components. There are only two known Cu-Fe oxides in nature (delafossite $Cu^{1+}Fe^{3+}O_2$ and cuprospinel $Cu^{2+}Fe^{3+}{}_2O_4$), and their stoichiometries and crystal morphology did not match the characteristics of this mineral. The following roentgen study showed that an X-ray line set corresponded to the synthetic Cu_2FeBO_5 compound, which is unknown in nature (analyst D. Belakovsky, Fersman Mineralogical Museum). The abundance of gold crystals is high, comprising tiny angular gold platelets, which were found on every grain of Cu-Fe borate examined by SEM (Fig. 7C-E). Surprisingly, native Au crystals occur only on the surface of this Cu-Fe borate, whereas associated tenorite lacks gold crystals.

According to EDS measurements composition of native gold is 100 % Au in all samples. No detectable Ag admixture was found in native gold particles although discrete Ag sulfide was observed intergrowing with tenorite unassociated with native gold (Fig. 7F).

3.3. Gold content in volcanic gases of the NTFE

During our 2013 fieldwork gas and condensate samples were taken in two points in the lava fields. Gas with a temperature of 1030 °C and its condensate were sampled from a 30 cm in diameter window above the running lava. Volcanic gas condensate was also sampled from a fracture with a temperature of 690 °C in an immediate vicinity to the sample Tol 0313 (Chaplygin et al., submitted), therefore, the composition of the condensate 690 °C should represent the most close proxy to composition of fluid from which gold-bearing sublimates precipitated.

The high-temperature 1030 °C volcanic gas is composed of (mol.%): 95.5 H_2O, 0.47 CO_2, 2.01 SO_2, 1.18 HCl, 0.34 HF (Chaplygin et al., submitted) that is within a range of gas compositions for subduction zone volcanoes (Aiuppa, 2009). The He isotopes indicate a MORB-type source for the 1030 ^oC gas and a high degree of air contamination in the 690 ^oC gas sample – because of this the latter was not analyzed for the major components. Oxygen and H isotopic data on the 1030 °C condensate ($\delta^{18}O$ = 6.35 ‰, δD = -32 ‰) also indicate the magmatic source whereas the 690 °C condensate shows the significant shift towards heavy oxygen isotope composition ($\delta^{18}O$ = 18.91‰, δD = -68.5‰).

The gas condensate taken at 1030 °C contains 3 ppb Au, 39 ppb Ag and 9.7 ppm Cu comparing to 16 ppb Au, 190 ppb Ag and 1180 ppm Cu in the 690 °C condensate. The 690 °C condensate is also extremely enriched with Cl as well as with alkaline and alkaline earth elements with respect to their content in the condensate of magmatic gas at 1030°C (Fig. 8).

Their content in the 690 °C condensate are 0.5 to 2 orders of magnitude higher than in the 1030 °C condensate up to 3260 ppm K, 2.6 ppm Ba, 1.2 ppm Ca, 1.7 ppm Rb, 1.2 ppm Pb, 0.8 ppm Cs and 135 ppb Sr. Highly-siderophile elements also show elevated abundances up to 33 ppb Pd, 21 ppb Rh, 0.4 ppb Ru and 0.4 ppb Os with respect to their contents in the 1030 °C condensate with 1 ppb Pd, 0.2 ppb Rh and the others being below ICP-MS detection limits (see Table 2 in Chaplygin et al., submitted). On the contrary, most of siderophile and chalcophile elements (Zn, Bi, Sn, Cd, In, Te and Mo) are relatively depleted in the 690 °C condensate with the exceptions of Pb, Se, Ag and Cu mentioned above (Fig. 8).

4. Discussion

4.1. Morphology and compositions of gold particles

All observations at Tolbachik, Colima (Taran et al., 2000), Kudriavy (Yudovskaya et al., 2006) and Erta-Ale (Zelenski et al., 2014) high-temperature fumaroles show that the first gold nuclei, i.e., the smallest particles recognizable under SEM, have euhedral morphology, made of platy and isometric crystals. Pure native gold is expected to crystallize from oxidized (SO_2>>H_2S) gas at temperatures up to 625 ^oC, and Au with Ag in solid solution likely forms at lower temperature. Ternary Cu-Au-Ag alloys, such as those found at Kudriavy and La Fossa (Fulignati and Sbrana, 1998), certainly, form from more reduced gas close to the primary magmatic fluid by composition at temperatures up to 870 ^oC. Transmitted electron microscopy showed that ternary alloys from Kudriavy are heterogeneous (Yudovskaya et al., 2006) possibly resulting from accretion (self-aggregation) of nanoparticles (or clusters) composed of binary Au–Ag and Cu-Au alloys. Accretion of much larger micron-sized particles is observed in the samples from Tolbachik although it is difficult to judge whether they nucleated from flowing gas or on the surface of sublimates. The observed variety of the microparticles and skeletal aggregates reflect the next sequence of events: primary nucleation, hitting and aggregation, and Oswald ripening or recrystallization.The anisotropic skeletal growth appears to be a characteristic for fumarolic native gold growing from low-density diluted fluids. The detailed discussion of the formation mechanism of elongated crystals, wires, whiskers and hollow crystals in gaseous medium can be found elsewhere (i.e. Givargizov, 1975; Symonds, 1993). It is a generally approved that formation of dendritic structure is a consequence of non-equilibrium growth and molecular anisotropy the where growth rates of various faces is kinetically controlled by adsorption and desorption from surrounding medium (Nittmann and Stanley, 1986). The etched rounded morphology of some crystals in the Tolbachik samples indicates a disequilibrium between gas unsaturated in gold and sublimates while crystallization of perfect crystals were supported by a local saturation and gas transport reactions.

4.2. Mechanism and timing of gold crystallization

Findings of gold minerals in fresh sublimates (Yudovskaya et al., 2006; this study) and in quartz tube experiments on volcanoes (Korzhinsky et al., 1996; Taran et al., 2000; Zelenski et al., 2014) indicate that their crystals can grow very fast within a few days or even hours. These promptly growing crystals appear to precipitate directly from hot gas via gas transport reactions - a natural occurrence of chemical vapor deposition (CVD). This process is widely used in industry to produce crystals and films, semiconductors and defect-free crystals. The fastest crystal growth during the CVD is provided by vapour-liquid-solid mechanizm (Givargizov, 1975). Growth occurs at contact between growing nuclei and thin supersaturated liquid layer whereas diffusion into this layer is controlled by thermal gradient which is a major factor of deposition at CVD. One of the first reports on CVD grown gold crystals (Schäfer, 1961) shows a photo of striking similarity to the natural crystals from fumaroles (Fig. 8). Schäfer (1961) summarized the main rules of precipitation from gas phase via gas transport reactions and showed that gold was deposited as a result of disproportionation:

$$\underset{T_1(900)}{Au_{solid} + Cl_{2gas}} \rightarrow \underset{T_2(700)}{AuCl_{2_{gas}}} \rightarrow Au_{solid}{}^{o} + AuCl_{4gas}.$$

The important features of gas transport reactions are 1) most metals and their various compounds (oxides, salts, sulfides, sulfosalts) can be transported; 2) crystallization temperature of metal compounds from gas is lower than that from a melt; 3) various gases such as halogens, hydrogen, oxygen, water and chlorides can be carriers; 4) an amount of gas carrier is small in comparison to an amount of transported solid; 5) compounds of the same element with different valence states can co-exist and intergrow (Shmulovich and Churakov, 1998; Yudovskaya et al., 2008); 6) parameters and morphology of growing crystals are controlled by parameters of the medium.

4.3. Gold content in gases

Experimental data on gold solubility indicate Au concentration less than 0.5 ppb in the H_2S–S–H_2O vapor systems at 300–360 ^oC, and Au volatility increases in the presence of water that is explained by increasing solvation of Au species (Zezin et al., 2011). Pokrovski et al. (2014) suggested that Au in low-density fluids forms complexes with the same ligands as in dense liquid, but the ligation number and redox state of Au might be different. It is known that in hydrothermal solutions Au solubility increases with increasing temperature that is accompanied by a regular change of the dominant species from $AuHS^o$ ($\pm AuOH^o$) to $AuHS^o + Au(HS)_2^-$ and to $AuCl_2^-$ above 500 ^oC and it depends of the fluid composition, Cl and S content and pH (Pokrovski et al., 2014). Hydrosulfide transport is expected to be negligible at highly oxidized

conditions of the Tolbachik active vents where H_2S was not detected in gas samples (Zelenski et al., 2014) and sublimate assemblages predominantly contains sulfates (including anglesite), halogenides and oxyhalogenides. The 1975-76 LTFE gold-bearing mineral assemblages do not contain sulfide compounds and form at highly oxidized conditions (Vergasova et al., 1982) suggesting that sulfide transport was impossible. The co-existence of mono- and bivalent Cu compounds also indicates an oxidation state near the Cu_2O/CuO buffer line with sulfur fugacity being in sulfate-ion field above the Ag/Ag_2S equilibrium. Extrapolating the growing stability of $AuCl_2^-$ with increasing temperature, which is shown for the oxidized solutions (Pokrovski et al., 2014), into the temperature field of high-temperature fumaroles (up to 1030 ^oC at Tolbachik), we can expect the highest Au solubility in the highest temperature magmatic gas due to enhanced chloride transport. The experiments by Hurtig and Williams-Jones (2014) showed that hydrated Au monochloride species played an important role in low density aqueous fluids with high HCl concentrations. Gold solubility in their experiments increases with increasing water vapour pressure and reaches 4.6 ppm at 400 °C and 297 bar that is significantly higher than any values found in fumarole condensates and similar to the high values measured in fluid inclusions (Pokrovski et al., 2014). Extrapolation of these new experimental data (Hurtig and Williams-Jones, 2014) allows to predict even higher solubility of Au at temperature between 400 and 600 ^oC with the hydrated Au monochloride $AuCl(H_2O)_y$ as the dominant gold species.

The predominant chloride transport is consistent with the composition of observed mineral assemblages although the role of SO_2 and F-bearing ligands in transport, deposition and dissolution of Au species is unresolved due to lack of experimental data. Given the predominant sublimate formation in a zone of interaction between hot gases and cold atmosphere, we suggest that deposition of gold resulted from decomposition of chloride complexes at a temperature barrier in the zone of sharp temperature gradient near the surface.

The high metal abundances in the 690 ^oC condensate is an artifact resulted from evaporation of water during forced gas pumping at sampling and can not be considered as representative for the volcanic gas composition. An initial gas parental for the condensate was formed at mixing between predominant meteoric water (evaporated snow, see Edwards et al., 2014) and a magmatic end-member as followed from the stable isotope systematics (Fig. 10). We estimate the initial Au content in gold-bearing fluid being less than ~2 ppb in terms of the supposed proportion of magmatic gas and snow. The contrasting behavior of the geochemically different groups of elements at evaporation could be explained by bonding with the different ligands and their different volatilities at oxidized conditions.

Our data on Au abundance in 2012-13 Tolbachik condensate are similar the data on Au abundance in alkaline solution of the vacuumed Giggenbach bottle from the same point (7 ppb

Au; Chaplygin et al., submitted) and average values (5 ppb Au) reported by Zelenski et al. (2014). The variations are likely related to heterogeneous distribution of metals. However, they also may reflect losses of volatile compounds during open-system sampling and difficulties of recovery from a sulfur-rich ultra-acid condensate during analysis. As a result of the losses, the measured and reported concentrations in the 1030 ^{o}C condensate likely represent a minimum estimate of metal concentrations in vapor. On the other hand, the enrichment of the 690 °C condensate showed that uncontrolled evaporation at sampling can result to the disproportional selective element losses and enrichment that is difficult to recognize unless isotope data are provided.

The comparison of the natural Au abundances with the experimental data on Au solubility suggest that sublimate minerals can precipitate from the gas phase even at very low metal concentrations which may be well below the saturation level. The fast deposition occurs at achievement of local saturation within the heterogeneous gas mixture and can be replaced by the etching up to complete dissolution by chemically aggressive fluids. The transport and deposition of gold can be described within the same gas transport reaction when solid reacts at high temperature with a gas to form a volatile compound that decomposes into solid by the reverse reaction on cooling.

5. Conclusions

New findings of native gold in sublimates sampled on lava flows during 2012–13 Tolbachik Eruption confirm the ability of low-density (gaseous) fluids to effectively transport and deposit Au. Observations of micron-sized crystals of native gold imply rapid *in situ* nucleation and accretion with the following euhedral and skeletal growth. Gas transport reactions are considered to be the major mechanism for the native Au precipitation from high-temperature volcanic gases with the Au content in the range from 2 to 7 ppb.

Acknowledgements

The field expeditions were organized by A. Belousov and M. Belousova. The work could not be performed without professionalism of Vityaz-aero helicopter pilots. We thank Y. Taran and P. Kartashov for fruitful discussion and appreciate the help of M.V. Kuznetsova, I.G. Griboedova and D.I. Belakovsky in mineral analysis. Constructive reviews and suggestions by Gleb Pokrovski and Stuart Simmons greatly improved the manuscript. This study and field trips were supported by RFBR (project 14-05-00874).

References

Aiuppa A., 2009. Degassing of halogens from basaltic volcanism: insights from volcanic gas observations. Chem. Geol. 263: 99–109.

Belousov A., Belousova M., Edwards B., Volynets A., Melnikov D. 2015. Overview of the precursors and dynamics of the 2012–13 basaltic fissure eruption of Tolbachik Volcano, Kamchatka, Russia. J. Volcanol. Geotherm. Res. (this volume).

Chaplygin I.V., Lavrushin V.Y., Dubinina E.O., Bychkova Y.V., Inguaggiato S. Geochemistry of volcanic gas at 2012–13 Tolbachik eruption, Kamchatka, subnitted.

Edwards B., Belousov A., Belousova M. 2014. Propagation style controls lava-snow interactions. Nature Comm., 5666: 1–5. DOI: 10.1038/ncomms6666.

Fulignati P., Sbrana A. 1998. Presence of native gold and telluriumin the active high-sulfidation hydrothermal system of the La Fossa volcano (Vulcano, Italy). J. Volcanol. Geotherm. Res. 86: 187–198.

Giggenbach W.F. 1975. A simple method for the collection and analysis of volcanic gas samples. Bull. Volcanol. 39: 132–145.

Givargizov E.I. 1977. Growth of crystal whiskers and lamellas from vapor. Nauka, Moscow. 180 p. (in Russ.).

Hedenquist J.W., Aoki M., Shinohara H. 1994. Flux of volatile and ore-forming metals from the magmatic-hydrothermal system of Satsuma Iwojima volcano. Geology 22: 585–588.

Henley R.W., Berger B.R. 2013. Nature's refineries – Metals and metalloids in arc volcanoes. Earth-Sci. Rev. 125: 146–170.

Hurtig N.C., Williams-Jones A.E. 2014. An experimental study of the transport of gold through hydration of AuCl in aqueous vapour and vapour-like fluids. Geochim. Cosmochim. Acta 127: 305–325.

Karpov G.A., Vergasova L.P., Kardanova O.F. 2003. Gold in products of postmagmatic processes in the transitional continent-ocean zone (Kamchatka). In: Geodynamics, magmatism and minerogenesis of the Northern Pacific continental margin. Magadan. NESC FEB RAS. pp. 176−179. (in Russ.).

Korzhinsky M.A., Tkachenko S.I., Bulgakov R.F., Shmulovich K.I. 1996. Condensate compositions and native metals in sublimates of high temperature gas streams of Kudriavyi volcano, Iturup Island, Kuril Islands. Geochem. Int. 34: 1175–1182.

Kouzmanov K., Pokrovski G.S. 2012. Hydrothermal controls on metal distribution in porphyry Cu(–Au–Mo) systems. Soc. Econ. Geol. Spec. Publ. 16: 573–618.

Large Tolbachik Fissure Eruption. Kamchatka 1975–1976. 1984. Fedotov S.A. (editor). Nauka, Moscow. 638 p. (in Russ.).

Meeker K., Chuan R., Kyle P.R., Palais J. 1991. Emission of elemental gold particles from Mount Erebus, Ross Island, Antarctica. Geophys. Res. Lett. 18: 1405–1408.

Morgan J.W., Higuchi H., Takanashi H., Hertogen J. 1978. Chondritic Eucrite parent body – inference from trace elements. Geochim. Cosmochim. Acta 42: 27–38.

Nittmann J., Stanley H.E. 1986. Tip splitting without interfacial tension and dendritic growth patterns arising from molecular anisotropy. Nature 321: 663-668.

Pokrovski G.S., Akinfiev N.N., Borisova A.Y., Zotov A.V., Kouzmanov K. 2014. Gold speciation and transport in geological fluids: insights from experiments and physical-chemical modeling. In: Garofalo P.S., Ridley J.R. (editors) Gold-transporting hydrothermal fluids in the Earth's crust. Geol. Soc. London Spec. Publ/ 402: 9–70. doi 10.1144/SP402.4.

Rudnick R.L., Gao S. 2004. Composition of the continental crust. In: Treatise on Geochemistry. Holland H.D. and Turekian K.K. (editors). Elsevier, Amsterdam. 3: 1–64.

Schäfer H. 1961. Chemische transportreaktionen. Verlag Chemie, Weinheim (Russ. translation: Mir, Moscow). 254 p.

Shmulovich K.I., Churakov S.V. 1998. Natural fluid phases at high temperatures and low pressures. J. Geoch. Explor. 62: 183–191.

Sortino F., Nonell A., Toutain J.P., Munoz M., Valladon M., Volpicelli G. 2006. A new method for sampling fumarolic gases: Analysis of major, minor and metallic trace elements with ammonia solutions. J. Volcanol. Geotherm. Res. 158: 244–256.

Symonds R.B. 1993. Scanning electron microscope observations of sublimates from Merapi Volcano, Indonesia. Geochem. J. 26: 337–350.

Taran Yu.A., Bernard A., Gavilanes J.-C., Africano F. 2000. Native gold in mineral precipitates from high-temperature volcanic gases of Colima volcano, Mexico. Appl. Geochem. 15: 337–346.

Ulrich T., Günther D., Heinrich C.A. 1999. Gold concentrations of magmatic brines and the metal budget of porphyry copper deposits. Nature 399: 676–679.

Vergasova L.P., Naboko S.I., Serafimova E.K., Starova G.L., Filatov S.K. 1982. Exhalative native gold. Dokl. Acad. Nauk USSR. 264: 201–204 (in Russ.).

Vergasova L.P., Starova G.L., Serafimova E.K., Filatov S.K., Filosofova T.M., Dunin-Barkovskii R.L. 2001. Native gold deposits from gas emanations of cinder cones produced by the 1975–1976 Great Tolbachik Fissure Eruption. Volcan. Seismol. 22: 493–504.

Williams-Jones A.E., Migdisov A.A., Archibald S.M., Xiao Z.F. 2002. Vapor-transport of ore metals. In: Hellmann R., Wood S.A. (editors) Water-rock interaction: a tribute to David A. Crerar. Geochem. Soc. Spec. Publ. 7: 279–305.

Yudovskaya M.A., Distler V.V., Chaplygin I.V., Mokhov A.V., Trubkin N.V., Gorbacheva S.A. 2006. Gaseous transport and deposition of gold in magmatic fluid: evidence from the active Kudryavy volcano, Kurile Islands. Miner. Deposita 40: 828–848.

Yudovskaya M. A., Tessalina S., Distler V. V., Chaplygin I. V., Chugaev A. V., Dikov Y. P. 2008. Behavior of highly-siderophile elements at magma degassing: a case study at the Kudryavy volcano. Chem. Geol. 248: 318-341.

Zelenski M.E., Fischer T.P., de Moor M.J., Bernard M., Zimmermann L., Ayalewd D., Nekrasov A.N., Karandashev V.K. 2013. Trace elements in the gas emissions from the Erta Ale volcano, Afar, Ethiopia. Chem. Geol. 357: 95–116.

Zelenski M., Malik N., Taran Yu. 2014. Emissions of trace elements during the 2012–2013 effusive eruption of Tolbachik volcano, Kamchatka: enrichment factors, partition coefficients and aerosol contribution. J. Volcanol. Geotherm. Res. 285: 136–149. http://dx.doi.org/10.1016/j.jvolgeores.2014.08.007.

Zezin D.Y., Migdisov A.A., Williams-Jones A.E. 2011. The solubility of gold in H_2O–H_2S vapor at elevated temperatures and pressures. Geochim. Cosmochim. Acta 75: 5140–5153.

Figure captions

Fig. 1. Schematic plan of lava flows and sampling sites in Tolbachik area. Volcanic and cinder cones, and tops of volcanoes are designated. Lava flows of 2012–2013 NTFE are shown in violet, 1975-76 lava flows of Northern breakthrough - in grey. Locations of sampling site (Tol 0313 and Tol 2714) and Cone II with gold occurrence are shown.

Fig. 2. Gold occurrence at Tolbachik cinder cones of 1975–76 LTFE Northern Breakthrough (sample Tol 76 7/90, cone II). (A) Fragments of brick-colored basaltic cinder with green and white sublimates. (B) Surface of the altered cinder, demonstrating the abundance and different morphology of native gold particles (Au). Rectangle designates area shown in C. (C) Gold platelet (Au) of complex shape. (D) Elongated platy crystals of native gold (Au). (E) Gold particles (Au) of irregular shape partially buried under salts. (F) twelve-sided platy gold crystal (Au). B–F - BSE images.

Fig. 3. Typical platy hexagonal and elongated crystals of native gold showing skeletal growth from 1975–76 LTFE (sample Tol 76 7/90, Cone II). (A) General view of separated crystals. (B) Skeletal platelet. (C) Incomplete skeletal platelet. BSE images, digital color.

Fig. 4. Diverse morphologies of exhalative gold crystals from 1975–76 Tolbachik cinder cones (sample Tol 76 7/90, Cone II). (A-F) Smooth aggregates of rounded crystals with signs of dissolution-precipitation. BSE images.

Fig. 5. Morphology of exhalative gold from 1975–76 Tolbachik cinder cones (sample Tol 76 7/90, Cone II). (A-D) Euhedral isometric crystals of diverse habit. (E) Native gold crystals inside and on a melanothallite aggregate. (F)Melanothallite aggregates overgrowing on wire-like crystal of native gold. BSE images.

Fig. 6. Native gold occurrences in roof of 2012–2013 NTFE lava flow (sample Tol 0313 collected in May 2013). (A) Fumarole incrustations with green Cu sulfates. (B) Inner surface of lava crust fragment (sample Tol 0313) covered with greenish colored Cu-rich sublimates. (C) Network-like aggregate of native gold lying on anglesite crystals. (D) Smooth morphology of an aggregate of gold crystals. BSE images.

Fig. 7. Mineral associations of native gold in sublimates of NTFE 2012–2013. (A) Intergrowth of anglesite ($PbSO_4$) and native gold (Au) (details of photo in Fig. 6C). (B) Native gold (Au, bright) and anglesite ($PbSO_4$) intergrowing with cyanochroite $K_2Cu(SO_4)_2*6H_2O$ (Cch) (untreated sample Tol 0313). (C) Druse aggregates of Cu-Fe borate (Cu_2FeBO_5) with numerous gold micrograins (Au) on surface (sample 2714). Rectangle designates area shown in D. (D) Disseminated euhedral gold platelets on druse-like aggregate of unidentified Cu-Fe borate (Cu_2FeBO_5) (sample Tol 2714). (E) Micron-sized triangular gold platelets (Au) on surface of unidentified Cu-Fe borate (Cu_2FeBO_5) (sample Tol 2714). (F) Silver sulfide (Ag_2S) on tenorite (CuO) (sample 2714). BSE images.

Fig. 8. Trace element compositions of volcanic gas condensates sampled at 1030 ^oC and 690 ^oC at 2012-13 NTFE. Elements are arranged into geochemical groups according to their relative enrichment in the 690 ^oC condensate with respect to the pristine magmatic gas. The sequence of elements in each group is determined by decreasing concentrations in the 1030 ^oC condensate.

Fig. 9. Morphologies of gold crystals grown by CVD (after Schäfer, 1961) demonstrating similarity to fumarolic gold crystals.

Fig. 10. Model of formation of the highly enriched 690 ^oC solution on the $\delta^{18}O$ vs δD plot. Mixing line between the isotope compositions of the pristine magmatic gas at 1030 oC ($\delta^{18}O$ = 6.35 ‰, δD = -32 ‰) and local snow ($\delta^{18}O$ = 17.68‰, δD = -127.5‰) is shown. The isotope composition of the 690 ^oC condensate ($\delta^{18}O$ = 18.91‰, δD = -68.5‰) forms at super-evaporation of a putative intermediate source on the mixing line with a probable composition within a range from -127 to –68 ‰ δD corresponding to 0 - 2 ppb Au. Evaporation during sampling results to enrichment in some elements (including at least 8-fold increase in Au) and heavy oxygen isotope although it does not affect the hydrogen isotope composition of the condensate (data are from Chaplygin et al., submitted).

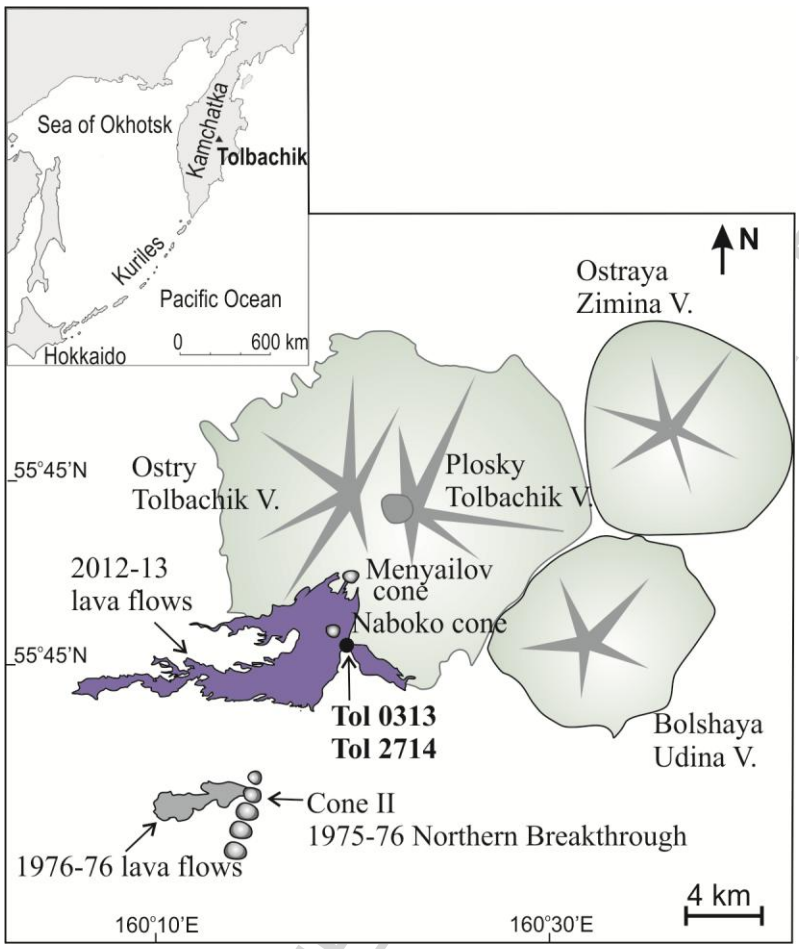

Figure 1

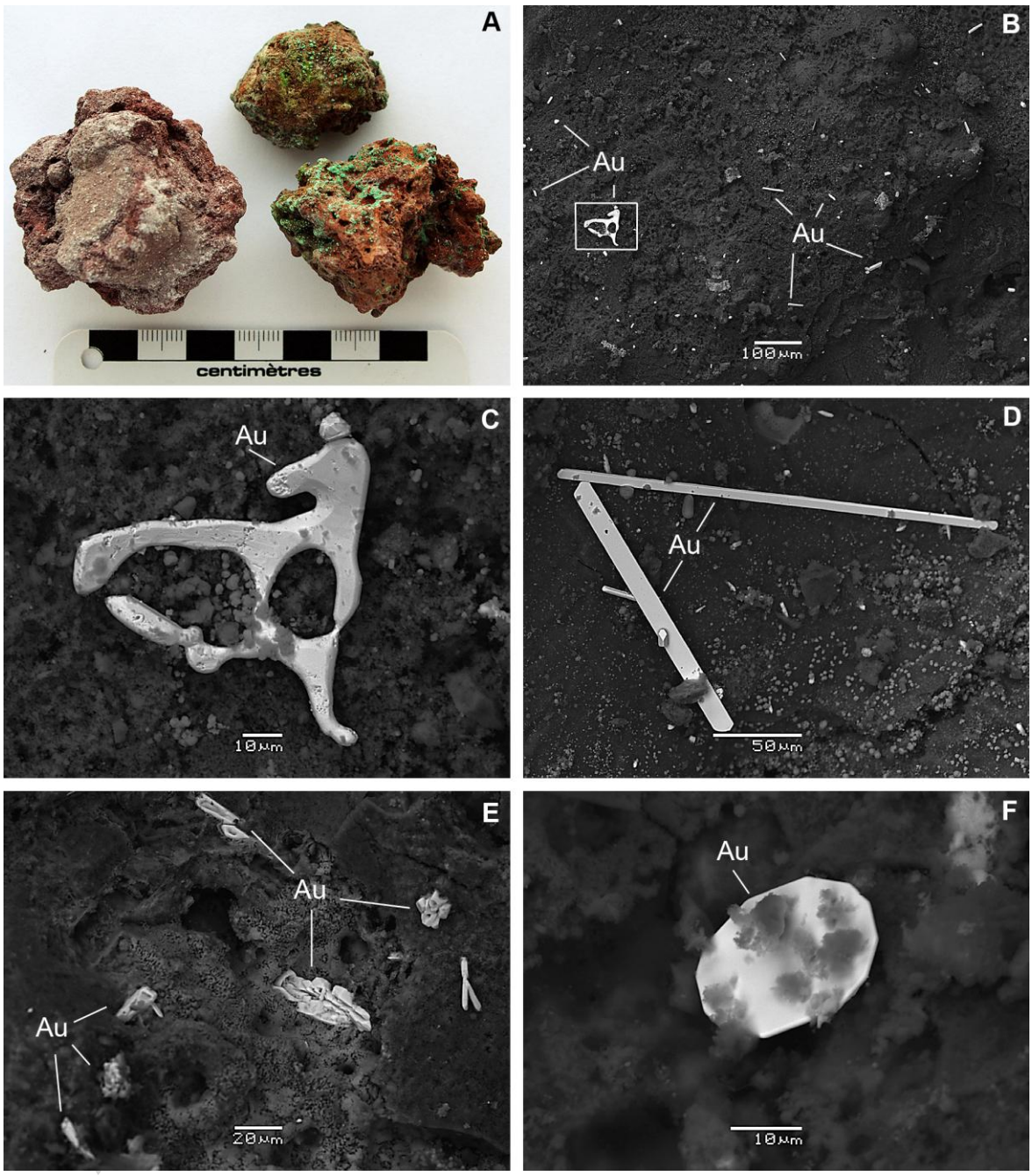

Figure 2

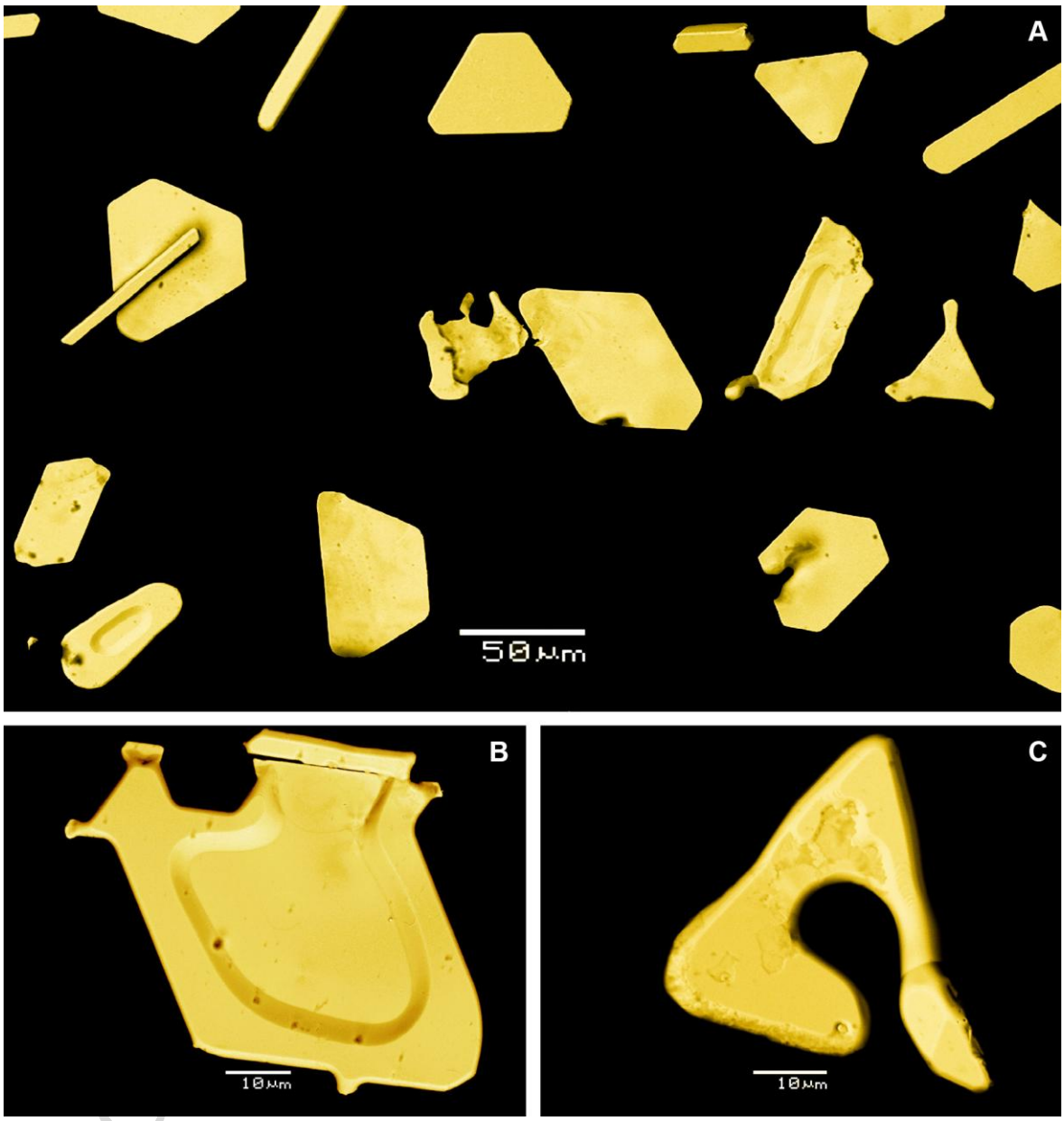

Figure 3

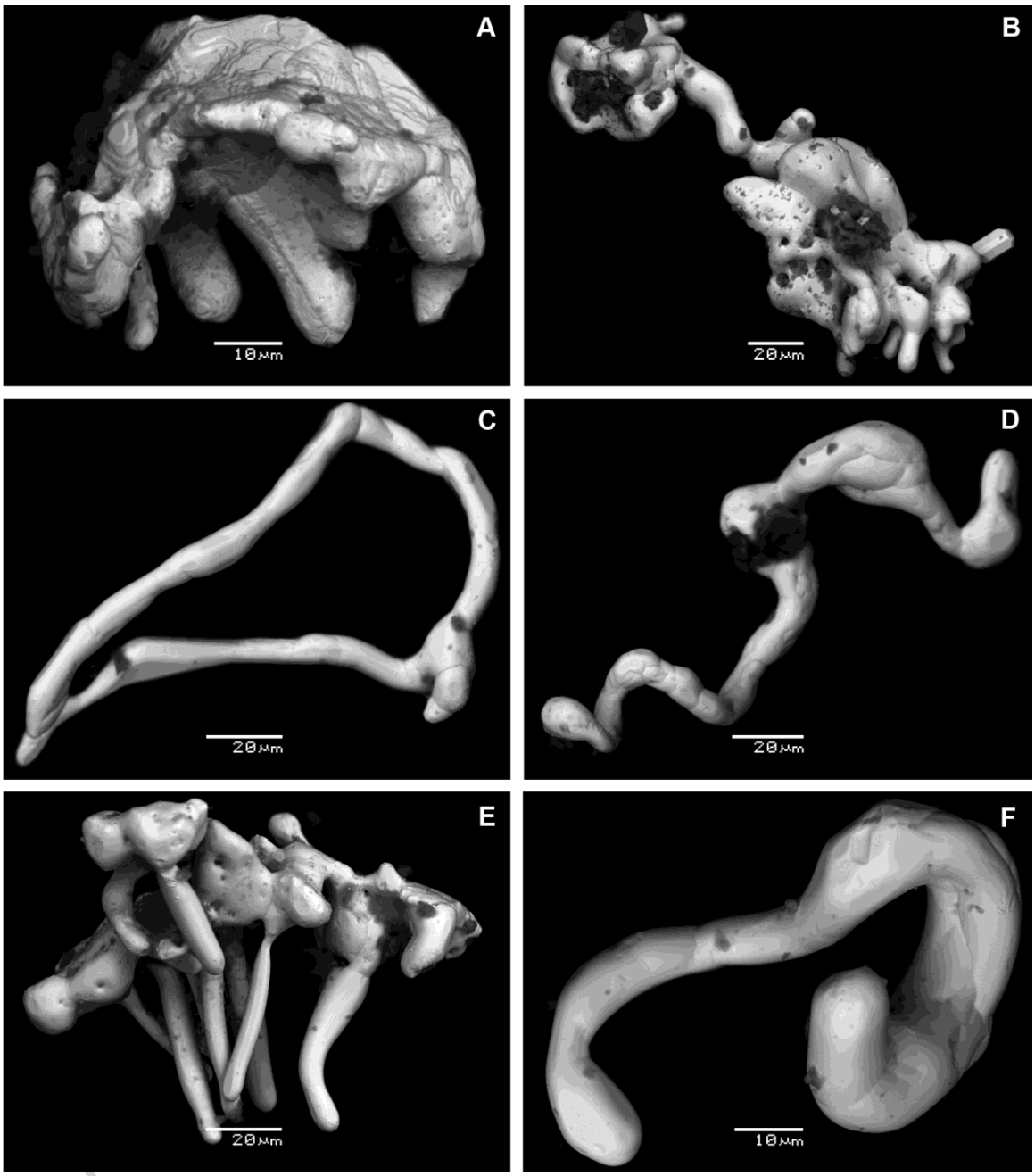

Figure 4

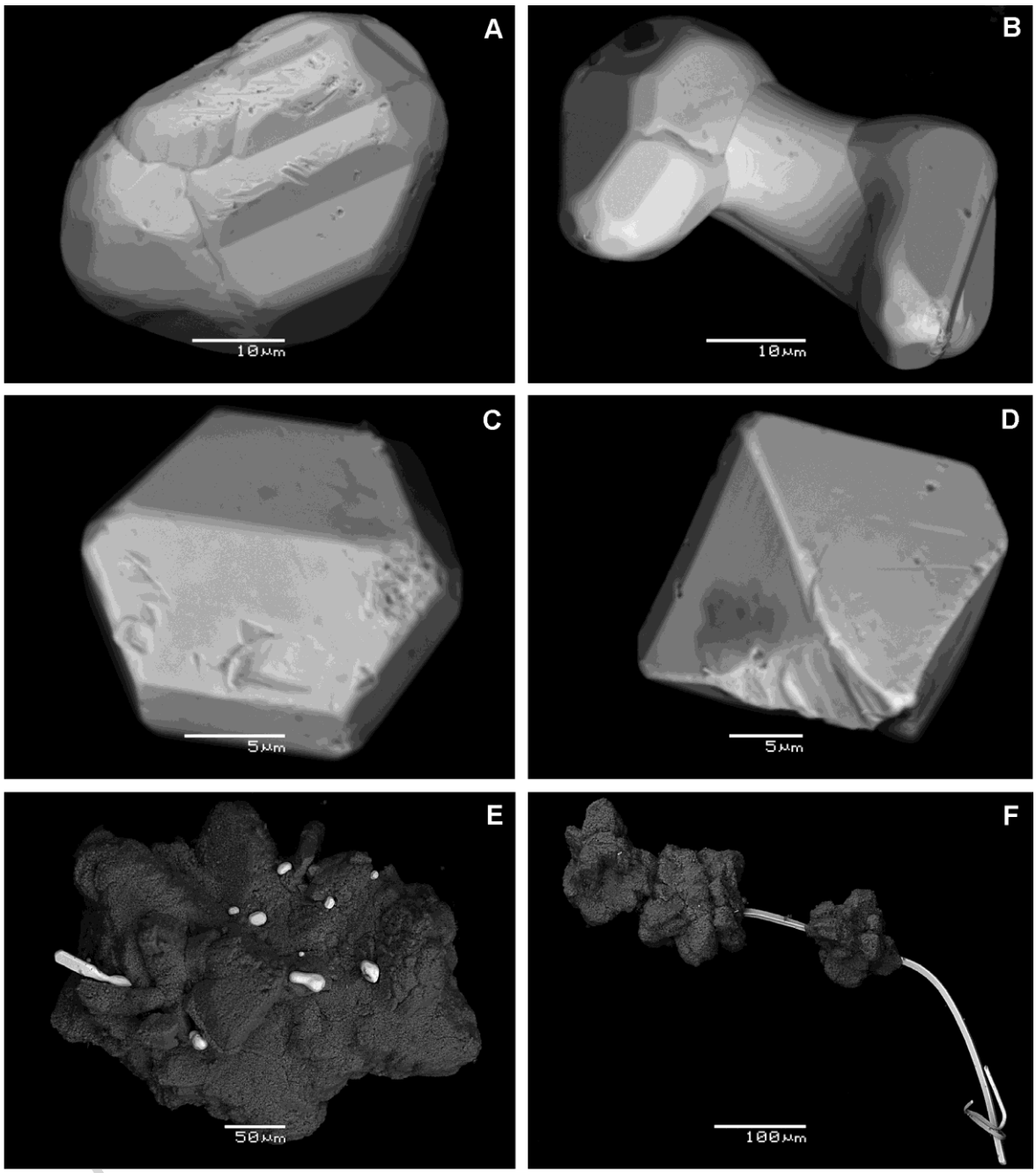

Figure 5

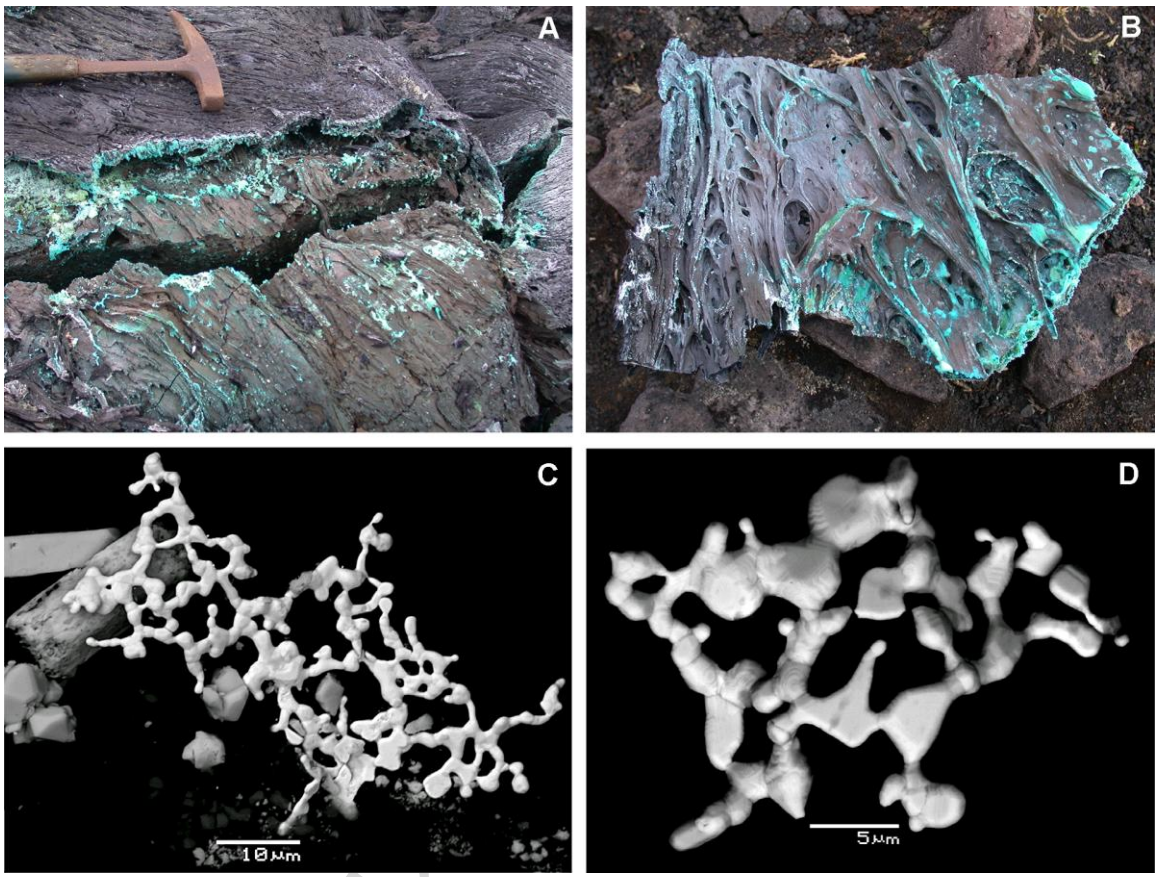

Figure 6

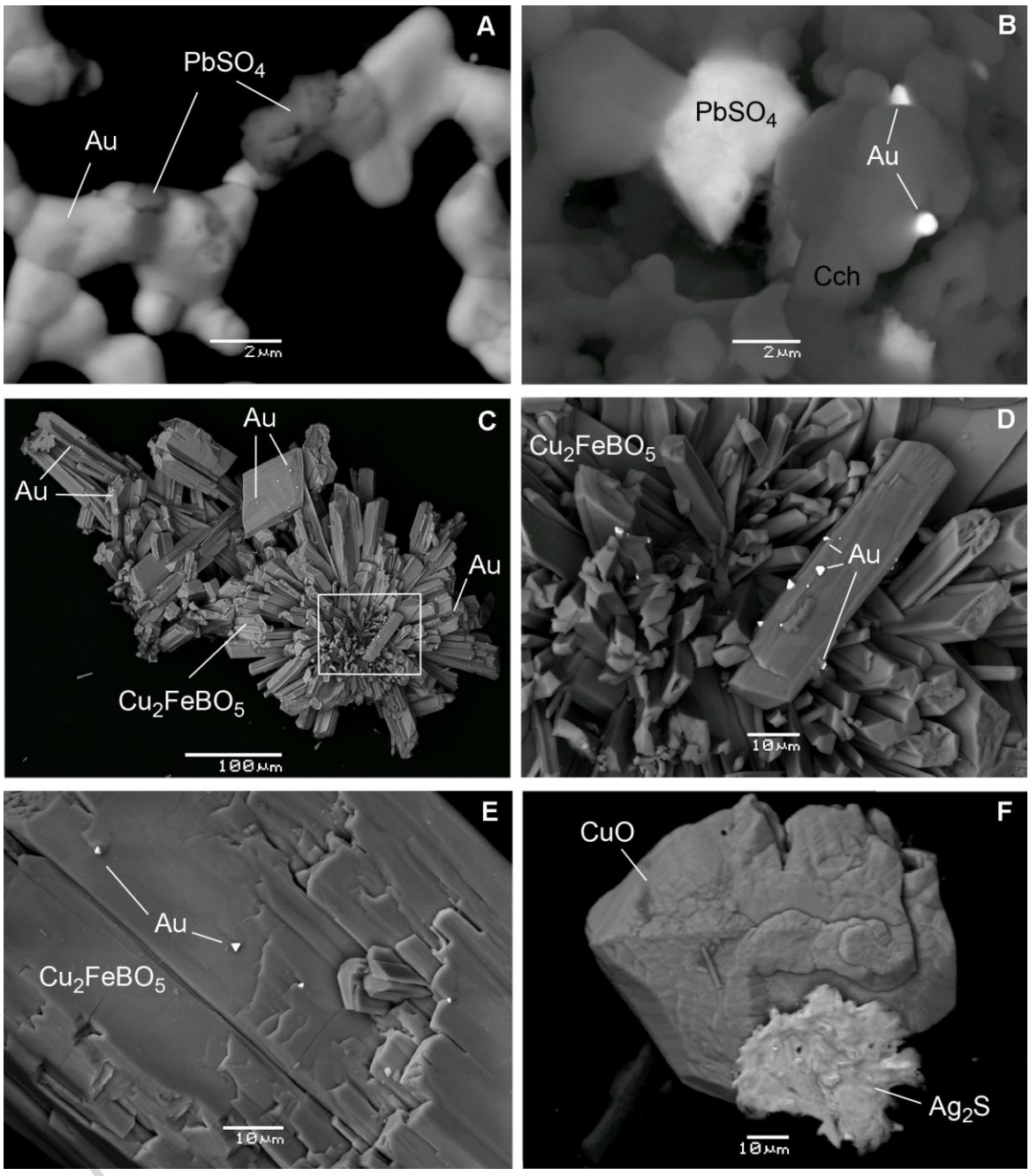

Figure 7

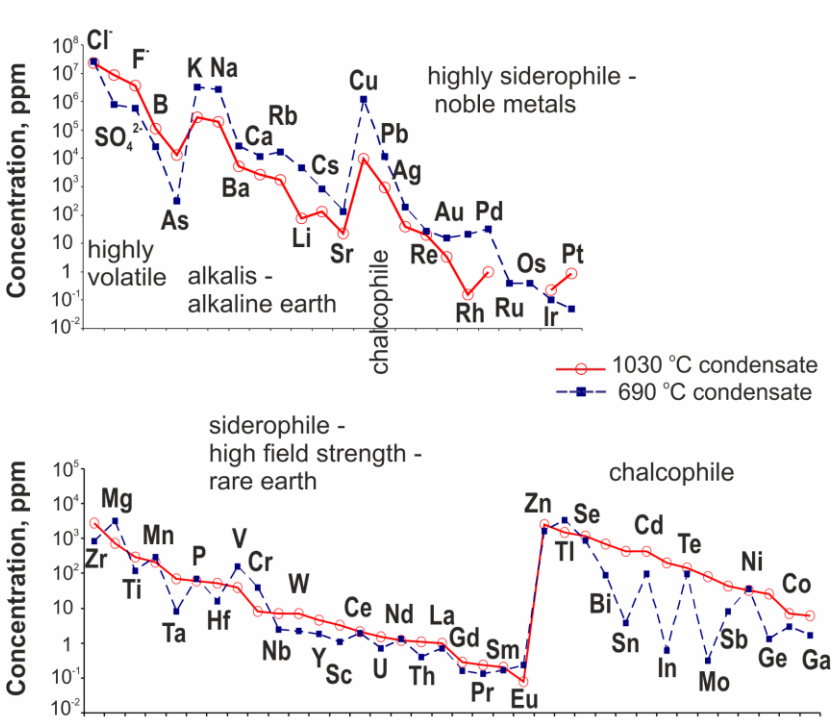

Figure 8

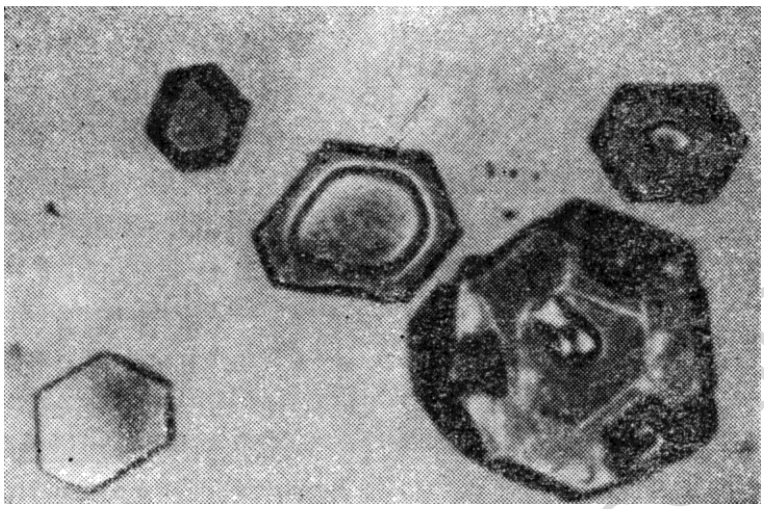

Figure 9

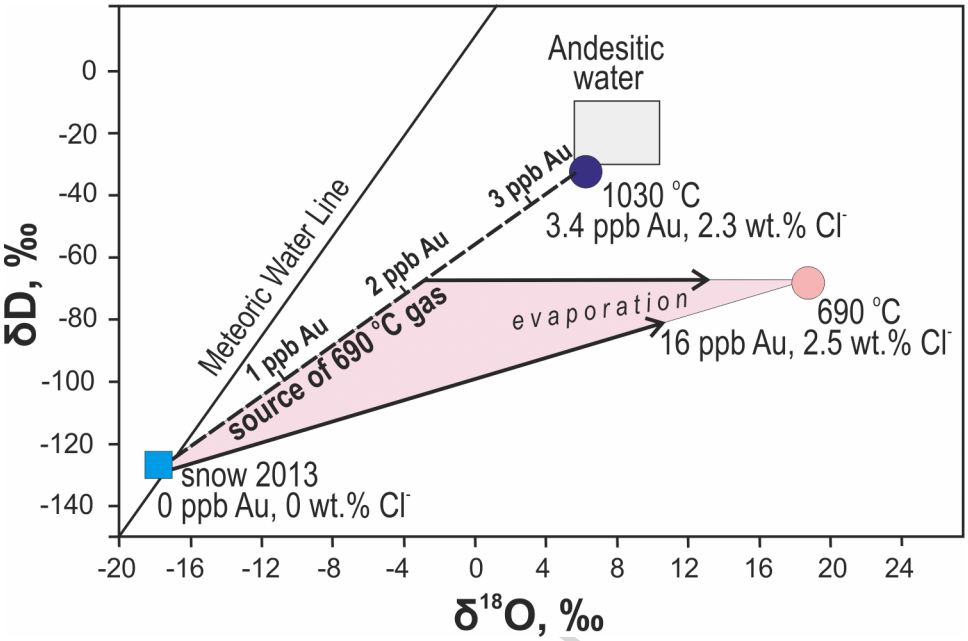

Figure 10

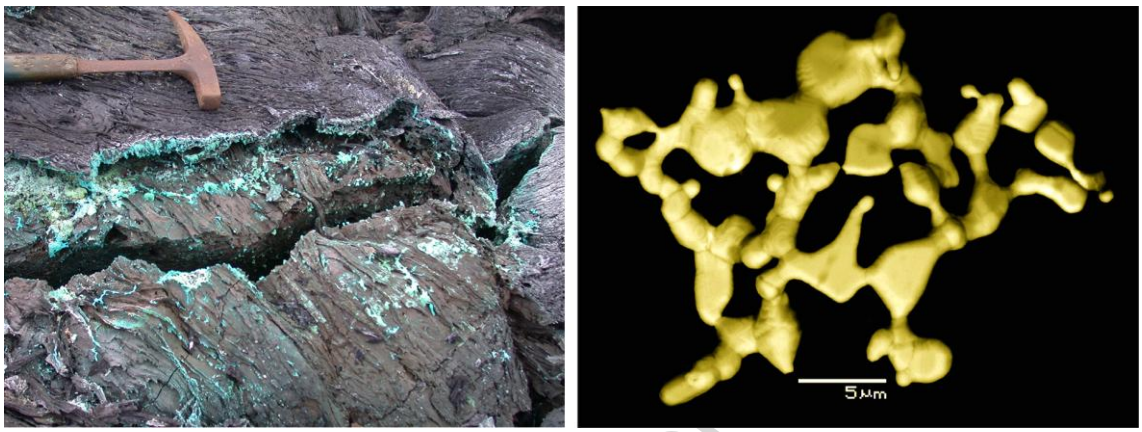

Graphical Abstract

Highlights

- Native gold crystallizes in the roof of the active lava flow at 2012–2013 NTFE.
- Sublimates precipitates from highly oxidized vapor at 690 ^{o}C.
- Euhedral rounded and skeletal gold crystals indicate heterogeneous state of fluid.
- The fumarolic gold occurrences illustrate an efficiency of gas transport mechanism.